

**THE INCLUSION OF OUT-OF-PLANE DISPLACEMENTS IN EIGENSTRAIN
RECONSTRUCTION PROCESS FOR ACCURATE MODELLING OF DISTORTION
IN IN740H WELDMENTS**



Fatih Uzun^{1,3}, Joris Everaerts¹, León Romano Brandt¹, Mehmet Kartal², Enrico

Salvati¹, Alexander M Korsunsky^{1,4,*}

¹MBLEM, Department of Engineering Science, The University of Oxford, Oxford, UK

²School of Engineering, University of Aberdeen, Aberdeen, UK

³fatihuzun@me.com, fatih.uzun@eng.ox.ac.uk

⁴alexander.korsunsky@eng.ox.ac.uk, * corresponding author

Authors' Accepted Manuscript

Published version in *Journal of Manufacturing Processes*

Volume 36, 2018, Pages 601–612

<https://doi.org/10.1016/j.jmapro.2018.10.047>

ABSTRACT

The purpose of the present study is to model distortion of Inconel Alloy 740H during the fabrication of welded components used for advanced ultra-supercritical technology by means of solving the inverse eigenstrain problem. The proposed model determines the distribution of two components of eigenstrain using two-dimensional displacement data obtained from high precision coordinate measurements. Input for the model is provided by the geometric characterisation of electric discharge machining (EDM) sectioned weld bead on plate sample, namely, the out-of-plane distortion of a transverse thin section across the weld line. The deplanation of the original sample is used for cross-validation using the contour method approach, modified recently by the present authors on the basis eigenstrain-based analysis. After determination of the distribution of eigenstrain components, residual stress and displacement calculations are performed in the whole body of as-welded and heat-treated plate models. Results are first verified using experimentally determined residual stress, displacement and distortion on the sectioned surfaces. In addition, 12 mm slices are cut from both model geometries and calculations are repeated using previously determined eigenstrain distributions. Measured distortions on the surface of bar models allowed a fourth term for verification of the eigenstrain distribution.

Keywords: weld distortion; residual stress; eigenstrain; reconstruction; iterative finite element modelling

1. INTRODUCTION

Advanced ultra-supercritical technology promises improvement in the efficiency of coal-fire based energy production by operating at higher temperature and pressure conditions.

Research in this technology focuses on the development of materials that provide high strength and corrosion resistance. Inconel Alloy 740H is a precipitation hardenable super-alloy that is appropriate for coal-fired steam turbines. Most common joining technique used for these materials is welding, but non-uniform expansion and contraction cycles of this process causes formation of residual stresses and distortion of components.

Power generation is accomplished at high temperature and pressure conditions where structural integrity is an important problem. According to Furtado and Le May [1] the principal deterioration mechanisms in power plants are creep damage, microstructure degradation, creep-fatigue, embrittlement, carburization, thermal shock, erosion, and high-temperature corrosion. Investigations on residual stress and its effect on structural deteriorations have vital importance for the service life of high technology alloys. Distortion is also an important problem caused by the welding process. It increases the error between designed and manufactured geometries and reduces dimensional accuracy.

Welding is a widely used technique for joining of industrial components made of similar or dissimilar materials. This process modifies the mechano-chemical state of materials similar to heat treatment techniques such as quenching, hot rolling and forging. Temperature gradients between the weld, heat affected zone and parent material cause formation of residual stresses in and around the weld region. Rapid heating results with volume expansion in weld zone while the resistance of surrounding cooler parts causes thermal stresses that may result in

yielding and rapid cooling ends with the shrink of the weld bead which is constrained by the cooler surrounding material. Finally, the process reaches a steady state where tensile stresses in the weld region are balanced by compressive stresses in the region further away from the weld [2].

Masubuchi [3] stated that the use of computers for the sake of analysis of welding process started in the late 1960s. Models for understanding the mechanism behind weld distortion are based on thermal elastic-plastic calculations, inherent deformations and analytical methods. Tian et al. [4] employed a thermo-mechanical finite element model for the purpose of investigation of transverse and angular distortions formed as a result of gas-tungsten-arc welding process at different operation condition defined by processing parameters which are voltage, current and speed. Another study that investigate the effect of processing parameters on distortion of electron beam welded titanium alloys using elastic-plastic calculations is performed by Li et al. [5]. Okano and Mochizuki [6] showed that the heat input of TIG welding process effect angular and longitudinal bending distortions monotonically and Bajpei et al. [7] investigated distortions as a result of gas-metal-arc welding of dissimilar AA5052 and AA6061 plates using a similar modelling approach. In spite of the fact that thermo-mechanical models are widely used for simulation of welding process, they consume high computation power. The first attempt to reduce the computation cost of these models proposed by Montevicchi et al. [8]. Authors proposed a new method to reduce computation time required for distortion prediction in wire arc additive manufacturing. The other method to reduce computation time is the use of inherent strains based on the fact that main source of the welding residual stress is the sum of non-elastic strains. The use of inherent strains for the purpose of investigation of weld distortion is proposed by Lou et al. [9]. Authors created inherent strains using the thermal cycles of welding process. The advantage of this method is

performing elastic analysis for determination of structural deformations that reduces the required computation power. Studies based on this method are summarised by Wang et al. [10]. According to Park and An [11], inherent strain method requires fine mesh distribution and high computation power. Authors proposed a new method that use mechanical forces instead of inherent strains that allow reduction in computation time when compared to thermal elastic plastic and inherent deformation methods.

Fitzpatrick and Lodini [12] summarized the studies that use X-ray and neutron diffraction techniques for determination of surface, sub-surface and in-volume residual stresses.

Longitudinal critically refracted (LCR) ultrasonic waves by Javadi et al. [13] and pulse echo ultrasonic waves by Uzun and Bilge [14] were also used for determination of in-volume residual stresses. However, these techniques have limitations in terms of cost and accuracy to perform in-volume residual stress mapping in large and non-uniform bodies. Prime [15] proposed a method based on contour measurements that provide a destructive but effective technique for determination of planar residual stress distribution. Several attempts have been done to verify this method using previously accepted residual stress measurement techniques. Kartal et al. [16], Prime et al. [17] and Traore et al. [18] used neutron diffraction method and Toparli et al. [19] and Zabeen et al. [20] used X-Ray diffraction method to compare residual stress calculations performed using contour measurements. Capturing high density surface displacement data allowed creation of detailed map of stress fields and emerged a new modelling approach. DeWald and Hill [21] used high density surface displacement data for determination of permanent plastic strain (eigenstrain) distribution and used that data for reconstruction of in-volume residual stresses with high accuracy. Kartal et al. [22] showed that the contour method and eigenstrain reconstruction process are effective on determination of residual stresses in welded thick components. However, previous studies on eigenstrain

reconstruction process were based on the assumption that weldments are uniform and longitudinal distribution of eigenstrain is constant within the body. Permanent plastic strains were determined to be distributed in the whole planar field that covers both weld zone and the edge parts far from the heat affected zone. This kind of distribution is able to provide good match with experimental fitting data, but it is far from reality, because welding residual stresses are expected to be formed as a result of permanent plastic strains formed in the weld zone.

The present authors [23] showed that eigenstrain reconstruction method can be used to identify the main source of welding residual stress by determining the eigenstrain distribution in and around the weld zone. Authors provided a new modelling technique that allows determination of volumetric eigenstrain distribution using a limited data set. According to the volumetric eigenstrain maps given in that study, compressive eigenstrains are collected in the heat affected zone. The crucial point about the distribution of eigenstrain is that they are determined accurately based on experimentally collected high density deplanation data. However, that study and all previously mentioned eigenstrain reconstruction attempts used only single component of displacement data, which is normal to cut surface, obtained by surface contour measurements. In this study, a second component of displacement, which is defined using measured weld distortion is included in the calculation of eigenstrain fields. This allowed determination of the distribution of permanent plastic strains in and around the weld beam that cause welding residual stress and weld distortion. The proposed method is applied to non-uniform as-welded and post-weld heat treated bead-on-plate specimens of Inconel 740H. Additional slice of cuts along the transversal direction are prepared to verify the predicted eigenstrain distribution in terms of distortion. The bar models also provided the possible longitudinal residual stress distribution in a uniformly welded body.

2. SPECIMEN MANUFACTURING

In order to model structural behaviour of materials used in ultra-supercritical power generation, as-welded and heat-treated specimens of Inconel Alloy 740H are prepared. Specimens are created using a non-uniform bead-on-plate design in spite of joining two parts. This design allows investigation of different stages of welding process and provides an understanding about the effect of the use of weld beams for the purpose of repairing steam turbine parts.

Inconel Alloy 740H is a super-alloy composed of chromium, 24.5 %, cobalt, 20.0 %, aluminium, 1.35 %, titanium, 1.35 % and niobium, 1.5 %, iron, carbon, manganese, molybdenum, silicon, copper, phosphorus, sulphur and boron elements at nominal ratios and nickel fulfils the balance. Dimensions of the plates, weld grooves and planes of measurements and cuts are illustrated in Figure 1. The thickness of plates is 12 mm while their length and width are 200 and 150 mm respectively. The slot for weld has approximately 12 mm width and 67 mm length at the top surface, 8 mm width and 63 mm length at its bottom section and 5 mm depth. After the machining of weld slots, samples are pre-weld annealed at 1107 °C for 1 hour with water cooling. Weld grooves are filled with three weld beads using a filler material that has the same composition with plates. Parameters of the tungsten inert gas (TIG) welding technique are given in Table 1. One of the samples is post weld heat treated (aged) at 800 °C for 4 hours with air cooling. Both samples are first cut from Plane A using EDM and slices with 12 mm length are created by cuts from Plane B after contour measurements on Plane A.

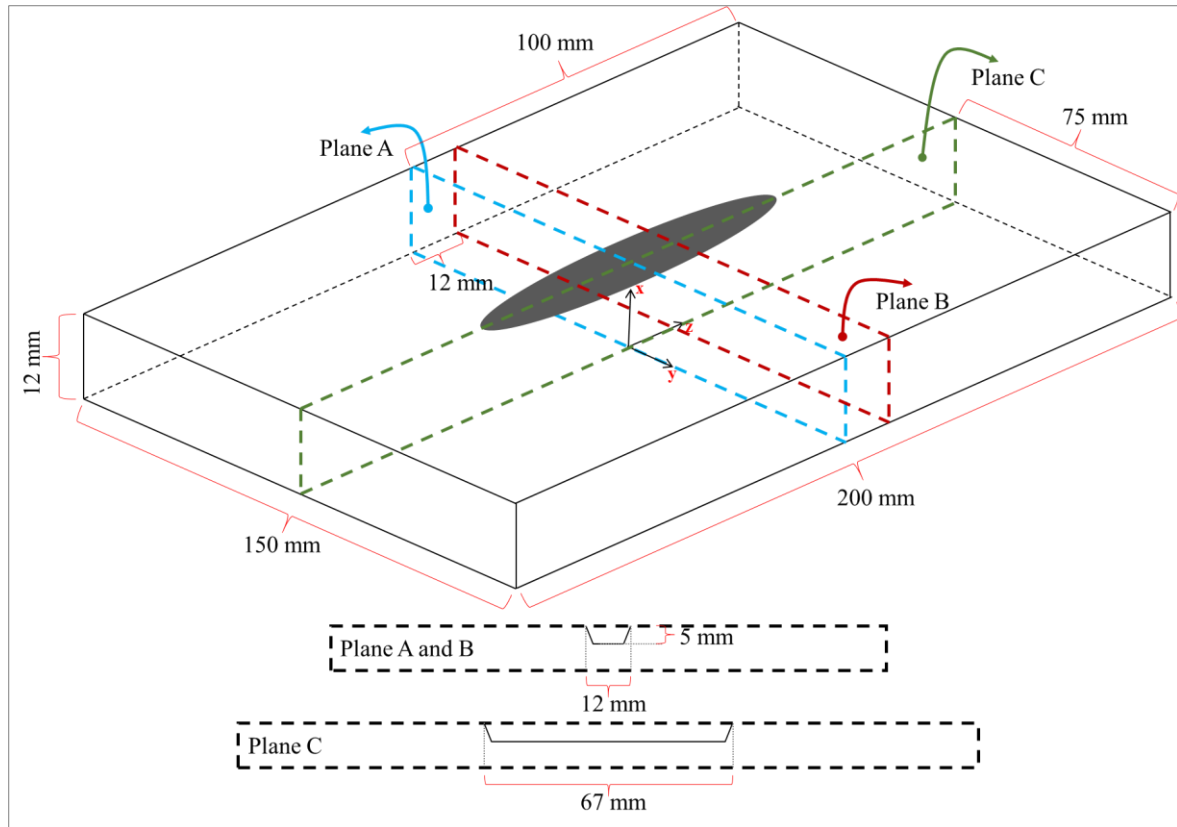


Figure 1. The 3D representation of the Inconel Alloy 740H specimens and dimensions.

Table 1. Parameters for TIG welding of as-welded (AW) and heat-treated (HT) specimens.

	Weld Pass 1		Weld Pass 2		Weld Pass 3	
	AW	HT	AW	HT	AW	HT
Current (A)	174.0	174.0	174.0	174.0	174.0	174.0
Voltage (V)	16.1	16.0	16.3	16.5	16.3	16.2
Travel Speed (mm/min)	163.0	136.4	152.4	111.5	134.3	123.4
Wire Speed (mm/min)	177.8	254.0	228.6	304.8	177.8	228.6

The importance of using this kind of specimen design is that the weld bead spans along one third of the length of the base plate. The sections without weld beam prevents full distortion subsequent to application of the weld beam. The preparation of a bar sample using a slice cut from Plane B eliminates the effect of un-welded welded sections on weld distortion. It is

assumed that EDM cutting process does not create plastic deformations on the cut surface. Accordingly, it can be stated that eigenstrains in the bar model are the eigenstrains formed during the welding process.

3. THE MULTI-COMPONENT AND MULTI-DIMENSIONAL EIGENSTRAIN MODEL

The contour method allows quantification of residual stresses by correlating experimentally measured displacement data with stress. The experimental data required for stress calculations are obtained using coordinate measuring machine (CMM) on two surfaces created by EDM sectioning process. In this study, the displacement data obtained as a result of destructive process are transferred to an elastic finite element model for residual stress calculation according to the principle of superposition which states that residual stresses are relaxed elastically on the surface of cut. This model simulates the conditions before the cutting process by applying the inverse of processed displacement data.

In this study, as-welded and heat-treated specimens are cut from Plane A using AgieCharmilles CUT 20 P Wire EDM cutting machine at cutting speeds of 2.0 and 2.2 mm/min respectively. The wire diameter for cutting Inconel alloy 740H is determined to be 0.25 mm. Crysta Apex C 3D CNC CMM is used for contour measurements on both surfaces of cuts from Plane A. Density of the measurements are determined to be 200 measurement points per mm². After the contour measurements, perimeters of all four parts around the cut surface are determined by coordinate measurements. A second cut is created from Plane B of both specimens, but contour measurements are not performed on the new cut surface. Only distortion measurements are performed on both sides of 12 mm slices.

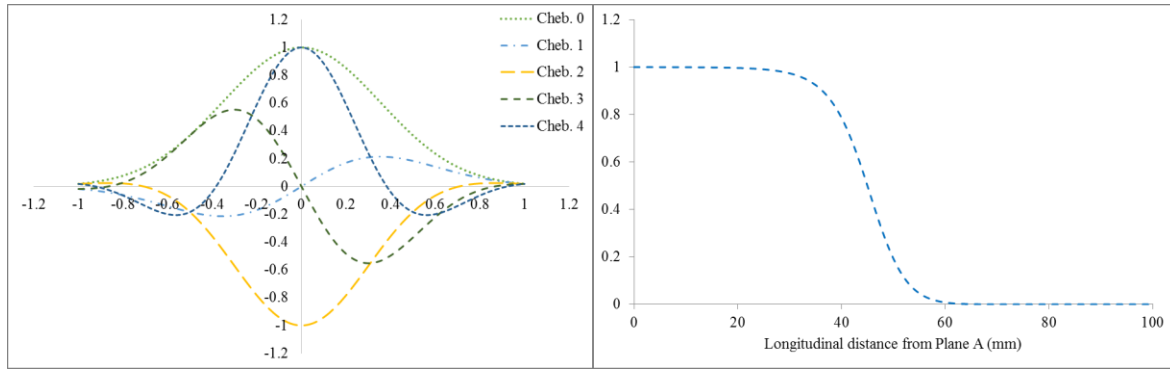


Figure 2. Chebyshev functions up to 4th order combined with Gauss function (left) and the knee function modified for determination of longitudinal weld length (right).

Residual stresses are the stresses that are accommodated in a material without any external load. Determination of these stresses is a challenging task while understanding their distribution in a material has vital importance. Ahn et al. [24] stated that it is impossible to get a full map of six components of residual stress in engineering components using currently available expensive and time consuming methods. For this purpose, thermal elastic plastic finite element models are widely used but these models require careful determination of heat source geometry, temperature dependent material properties and dimensions of the material. When the complexity of plasticity and details of thermal model are included, high number of unknowns causes the results of these models to highly deviate from experimental verifications. In order to deal with these difficulties, eigenstrain reconstruction method was developed that combines accuracy of high density experimental data from contour measurements with elastic finite element models. The idea behind this approach is using the main source of residual stresses, eigenstrains, which is first introduced by Mura [25], for calculation of residual stresses. Korsunsky [26] presented examples of this method in various applications.

In this study, planar distribution of eigenstrain is determined using a combination of Chebyshev polynomial functions up to 4th order and Gauss function, however, non-uniform bead-on-plate specimen design created a requirement of determination of eigenstrain variations along the longitudinal direction that is satisfied by using the knee function which was developed by Korsunsky [27]. Chebyshev functions up to 4th order and Gauss function and the shape of modified knee function is illustrated in Figure 2. Previously, the present authors [23] showed that multi-component iterative process provided highly accurate results with high quality of fit when distribution sizes were determined to be 80 mm for as-welded and 100 mm for heat-treated specimens of Inconel Alloy 740H. In this study, distribution of two components (ε_{yy}^* and ε_{zz}^*) of eigenstrain are determined using the same iterative process, that matches displacements in the direction of distortion and displacements normal to fitting surface with experimental measurements of distortion and displacement, and the same eigenstrain distribution sizes. The quality of fit of displacement and residual stress is analysed for all iteration steps using Equation 1 where Y_p is the displacement calculated eigenstrain reconstruction method and X_p is the measured and averaged displacement using contour method at the p^{th} measurement point.

$$MSE = \frac{1}{n} \sum_{p=1}^r (Y_p^2 - X_p^2) \quad (1)$$

The zz -component of eigenstrain is the primary driving force on reconstruction of residual stress field. In order to get better fit of residual stress, it was concluded that yy -component of eigenstrain should be included in the process of reconstruction of residual stress fields. The multi-component iterative model allowed reconstruction of residual stresses on the surface of cut precisely and reliable prediction of residual stresses in the whole body. However, that

model was based on single component of experimental data. z-component of displacement measured on the surface of cut was matched with experimentally calculated displacements. In this study, x-component of displacements is included for matching calculated weld distortion with experimentally measured weld distortion.

The second component of eigenstrain is included based on a physically-based assumption that two components of eigenstrain are proportional with a fixed coefficient. In order to determine coefficients of each component of eigenstrain, which are α for ε_{yy}^* and β for ε_{zz}^* , an iterative solution process was developed. Formulation of this approach is given in Equation 2.

$$\varepsilon^* = \alpha \begin{bmatrix} 0 & 0 & 0 \\ 0 & \varepsilon_{yy}^* & 0 \\ 0 & 0 & 0 \end{bmatrix} + \beta \begin{bmatrix} 0 & 0 & 0 \\ 0 & 0 & 0 \\ 0 & 0 & \varepsilon_{zz}^* \end{bmatrix} \quad (2)$$

Separate components of eigenstrain are determined as the sum of linear combinations of unknown polynomial series with same coefficients.

$$\varepsilon^*(x, y) = \alpha \left[\sum_{l=1}^{(m+1)(n+1)} A_l F_l(x, y) \right] + \beta \left[\sum_{l=1}^{(m+1)(n+1)} A_l F_l(x, y) \right] \quad (3)$$

where A_l is the unknown coefficient of l^{th} term of a series expansion of known basis functions, $F_l(x, y)$. The basis functions are used to generate planar distribution of eigenstrain by multiplying Chebyshev polynomial functions:

$$F_l(x, y) = P_{l,i}(x)P_{l,j}(y). \quad (4)$$

In this equation, i ranges from 0 to m and j ranges from 0 to n . Total of unknown coefficients of the basis functions, w , is determined as given below:

$$w = (m + 1)(n + 1) \quad (5)$$

The unknown coefficients are calculated using the measured average displacements by solving the elastic problem:

$$\{u\} = [C^I]\{A^I\} \quad (6)$$

where $\{u\}$ is a vector contains measured average displacements on the contour cut surface at r number of measurement points.

$$\{u\} = \left[u_1^x(x, y), u_2^x(x, y), \dots, u_{r_y}^x(x, y), u_1^z(x, y), u_2^z(x, y), \dots, u_{r_z}^z(x, y) \right]^T \quad (7)$$

The vector $\{A^I\}$ contains coefficients of w number of basis functions:

$$\{A^I\} = [A_1, A_2, \dots, A_w]^T \quad (8)$$

The model derived matrix, $[C^I]$, is composed of displacements obtained by solving basis functions, $F_l(x, y)$. Superscripts in $\{u\}$ vector and $[C^I]$ matrix represent displacement in xx and zz directions. The matrix used for multi-component iterative process has w number of columns for each polynomial term and $2r$ number of rows corresponding to each individual data point.

$$[C^I] = \begin{bmatrix} C_{1,1}^{xx} & \cdots & C_{w,1}^{xx} \\ \vdots & \ddots & \vdots \\ C_{1,r_y}^{xx} & \cdots & C_{w,r_y}^{xx} \\ C_{1,1}^{zz} & \cdots & C_{w,1}^{zz} \\ \vdots & \ddots & \vdots \\ C_{1,r_z}^{zz} & \cdots & C_{w,r_z}^{zz} \end{bmatrix} \quad (9)$$

In the next stage of iterative process, coefficients of independent solutions of yy and zz component of eigenstrain, $\{A^{II}\}$, are calculated using common coefficients of basis functions, $\{A^I\}$, by solving the elastic problem:

$$\{u\} = [C^{II}]\{A^{II}\} \quad (10)$$

The vector $\{A^{II}\}$ contains coefficients α and β for independent solutions.

$$\{A^{II}\} = [\alpha, \beta]^T \quad (11)$$

The model derived matrix, $[C^{II}]$, is composed of displacements obtained by solving $\varepsilon^*(x, y)$ for ε_{yy}^* and ε_{zz}^* independently which are done by setting α and β to zero while solving for ε_{zz}^* and ε_{yy}^* respectively.

$$[C^{II}] = [C_\alpha, C_\beta] \quad (12)$$

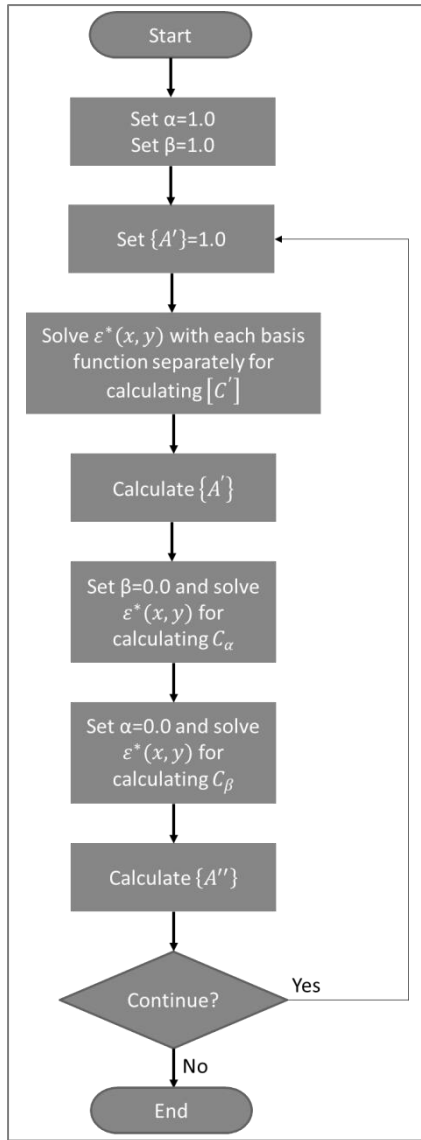


Figure 3. Flowchart of the iterative solution process [23].

The flowchart of the iterative solution process for the multi-component problem with two-dimensional displacement data is given in Figure 3. The solution is based on calculation of the coefficients of basis functions and the coefficients defined for each component of eigenstrain. Quantified quality of fit is compared with previous solution after each iteration and a decision is made on the continuation of the iteration process.

4. RESULTS

Contour measurements are performed with step size of 0.1 mm on both surfaces of cut planes of as-welded and heat-treated specimens. Displacement data is processed through the steps of alignment, interpolation, averaging, cleaning, smoothing, and flattening using computational tools of MATLAB engineering software. Details of data processing steps can be found in the study of Hosseinzadeh et al. [28]. Distribution of the processed displacement data of as-welded and heat-treated specimens are illustrated in Figure 4.

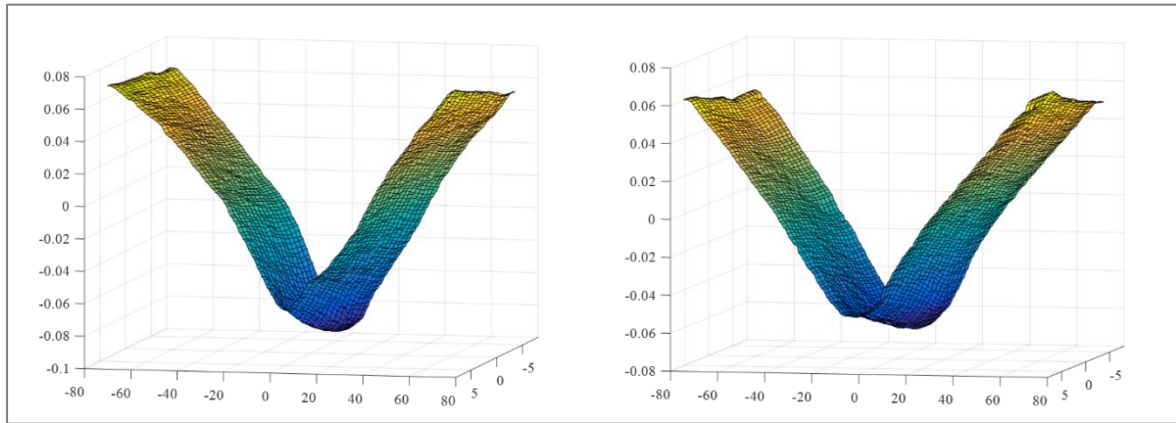


Figure 4. The processed displacement data of as-welded (*millimetres* - left) and heat-treated (*millimetres* - right) specimens used for calculations of the contour method and the multi-component and multi-dimensional eigenstrain model [23].

Iterative solution process is analysed for as-welded and heat-treated models using quantified quality of fit in terms of MSE of displacement. This model is based on fitting the calculated displacements and distortion with experimental measurements. Figure 5 illustrates MSE of displacement with respect to iteration number. Values are normalised to 100 to illustrate the percent of change. Results show that MSE of displacement decreases up to 6th iteration in as-welded specimen and then increases with a decreasing rate. According to these results,

optimum number of iterations is determined to be 6 which is the minimum number of iterations required to get best fit of displacement. Similar to the as-welded sample, MSE variation of displacement in heat-treated sample first decreases rapidly until the 5th iteration and then it increases. The number of iterations that provide minimum MSE are determined to be the optimum number of iterations for eigenstrain reconstruction process and the results provided by these solutions are used for further investigations.

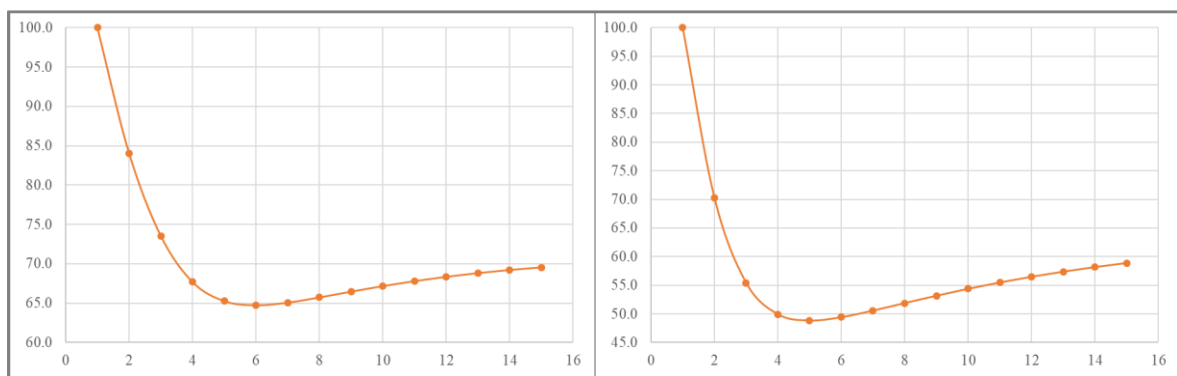


Figure 5. Quantified quality of fit in terms of MSE of longitudinal residual stresses and displacements normalised to 100 w.r.t number of iterations in as-welded (left) and heat-treated (right) sample models.

Multi-component iterative model assumes that two components of eigenstrain are locked in the same distribution while their magnitudes are determined with two different coefficients. The coefficients calculated for the as-welded and heat-treated models are given in Table 2. Figure 6 illustrates eigenstrain distribution in as-welded and heat-treated specimens after 6 and 5 iterations respectively. Two plots clearly represent the source of welding residual stress. Eigenstrain fields around the weld zone are surrounded by the fields with no permanent plastic strain. As it is expected, magnitude of compressive eigenstrains in the weld zone decreases because of heat treatment process. However, it should be mentioned that these are not the exact eigenstrain values. Real values of eigenstrains are determined by the finite

element model using coefficients of eigenstrain components during the calculation of structural deformations.

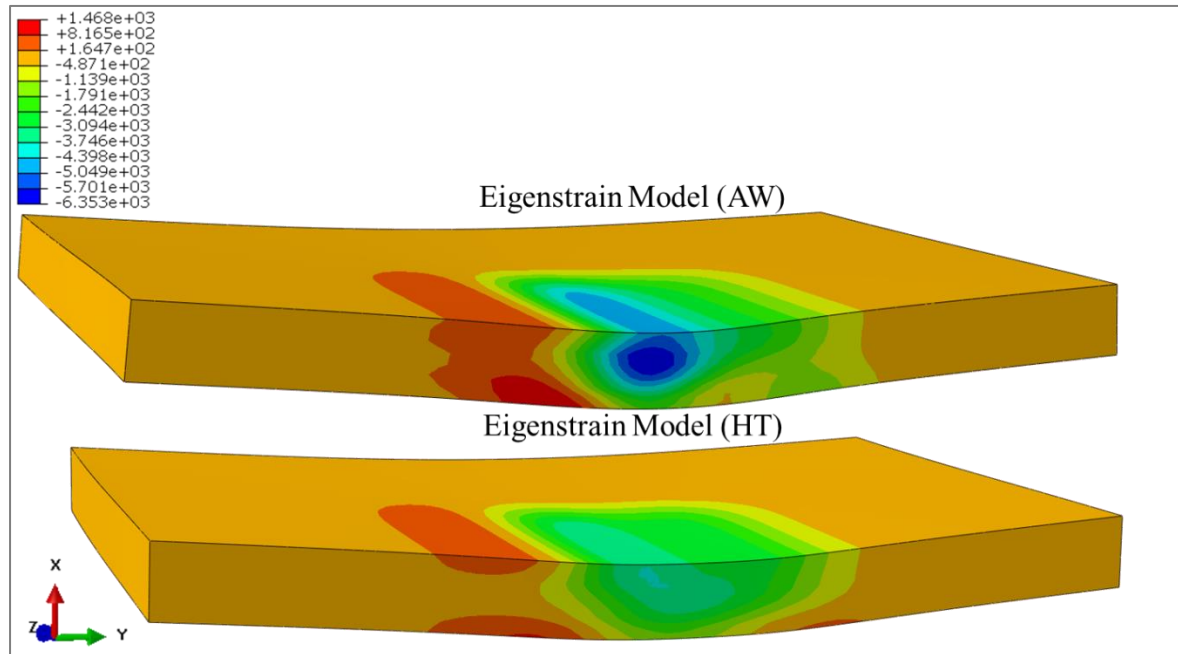


Figure 6. Distribution of eigenstrain, obtained using multi-component iterative eigenstrain reconstruction process, in as-welded and heat-treated models. Deformations are magnified with a scale factor of 10.

Table 2. Coefficients of eigenstrain components for as-welded and heat-treated models

	α	β
As-Welded	2.41×10^{-06}	4.55×10^{-07}
Heat-Treated	2.62×10^{-06}	3.62×10^{-07}

After determination of eigenstrain distributions and coefficient of eigenstrain components, longitudinal residual stress fields are calculated using finite element models whose results of as-welded plate and bar models are given in Figure 7. Eigenstrain model of the plate has a similar distribution of longitudinal residual stresses with the experimental calculations.

Although contour method is only sensitive to the distribution on the cut surface, eigenstrain model provides distribution of longitudinal residual stresses within the volume. Planar distribution of eigenstrains is used to calculate longitudinal residual stresses in bar model. In spite of the fact that they have the same eigenstrain distribution in xy-plane, magnitude of longitudinal residual stresses is different in bar model. Compressive longitudinal residual stresses at the edge parts along y-axis seem to be relaxed after the cutting process. The reason of the compressive residual stresses at the edge parts is implementation of un-welded part on distortion. When this implementation is removed, the bar sample is distorted freely and compressive longitudinal residual stresses away from the weld zone are relaxed. It should be emphasized that, the eigenstrain reconstruction model calculates longitudinal residual stresses in bar-model without inclusion of surface relaxations. According to this property of the model, it can be stated that the bar model represents longitudinal residual stress distribution in the case of a uniform weldment design.

Figure 8 illustrates longitudinal residual stress distribution in reconstructed plate and bar models of heat-treated specimen with experimental calculations of the contour method. Results show that the proposed model is capable of reconstruction of longitudinal residual stress fields in heat-treated specimen. As it is expected, heat-treated specimen has lower residual stress magnitudes than as-welded specimen. Like the bar model of as-welded plate, compressive longitudinal residual stresses away from weld zone in bar model of heat-treated plate are extinguished. The mechanism behind the results of as-welded model is also valid for the heat-treated model.

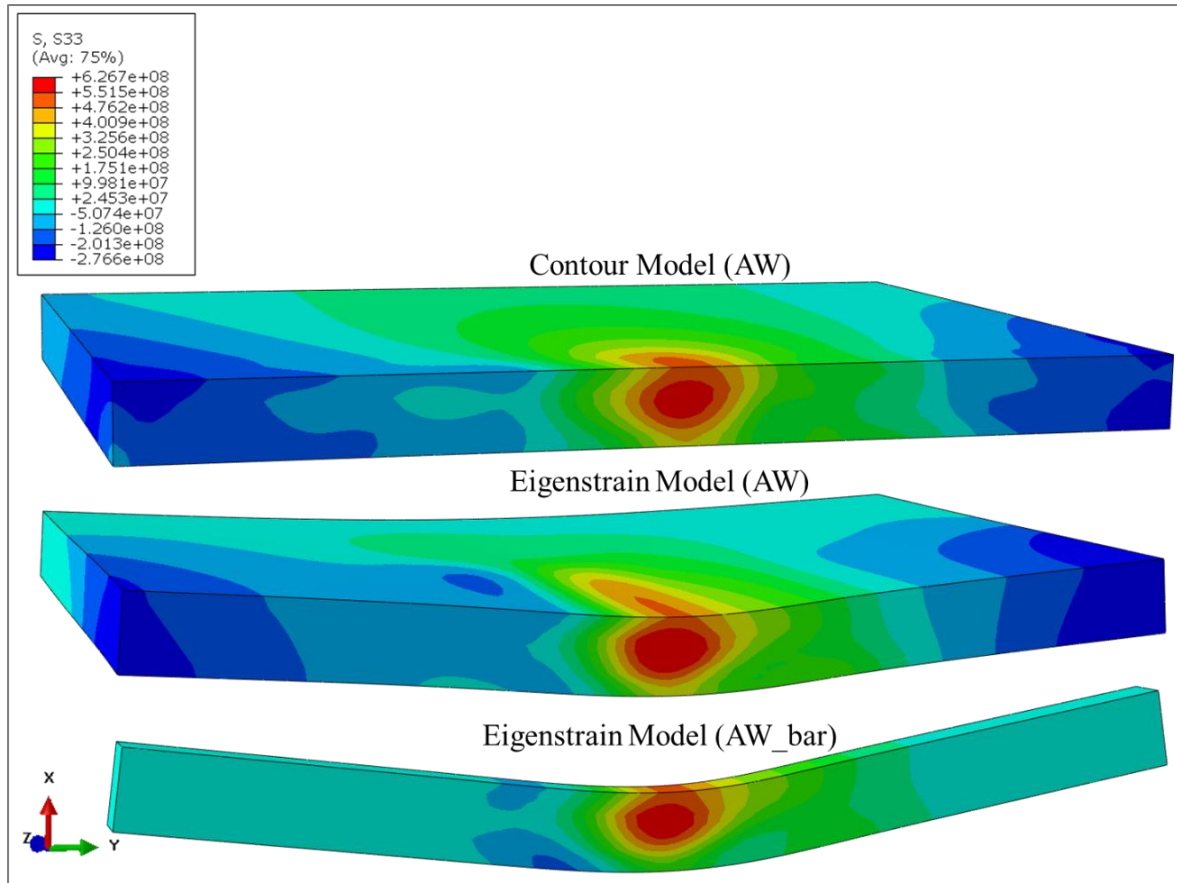


Figure 7. Distribution of longitudinal residual stress (Pa), obtained using eigenstrain reconstruction and contour methods, in as-welded plate and bar models. Deformations are magnified with a scale factor of 10.

Comparison of longitudinal residual stresses in bar models of as-welded and heat-treated specimens is given with a common legend in Figure 9. Results show that as-welded bar model has higher longitudinal residual stress magnitude and higher distortion than heat-treated bar model. Both models have low magnitude compressive longitudinal residual stress fields around the weld zone but longitudinal residual stresses at out of this zone are mostly zero up to the edge parts of the bar.

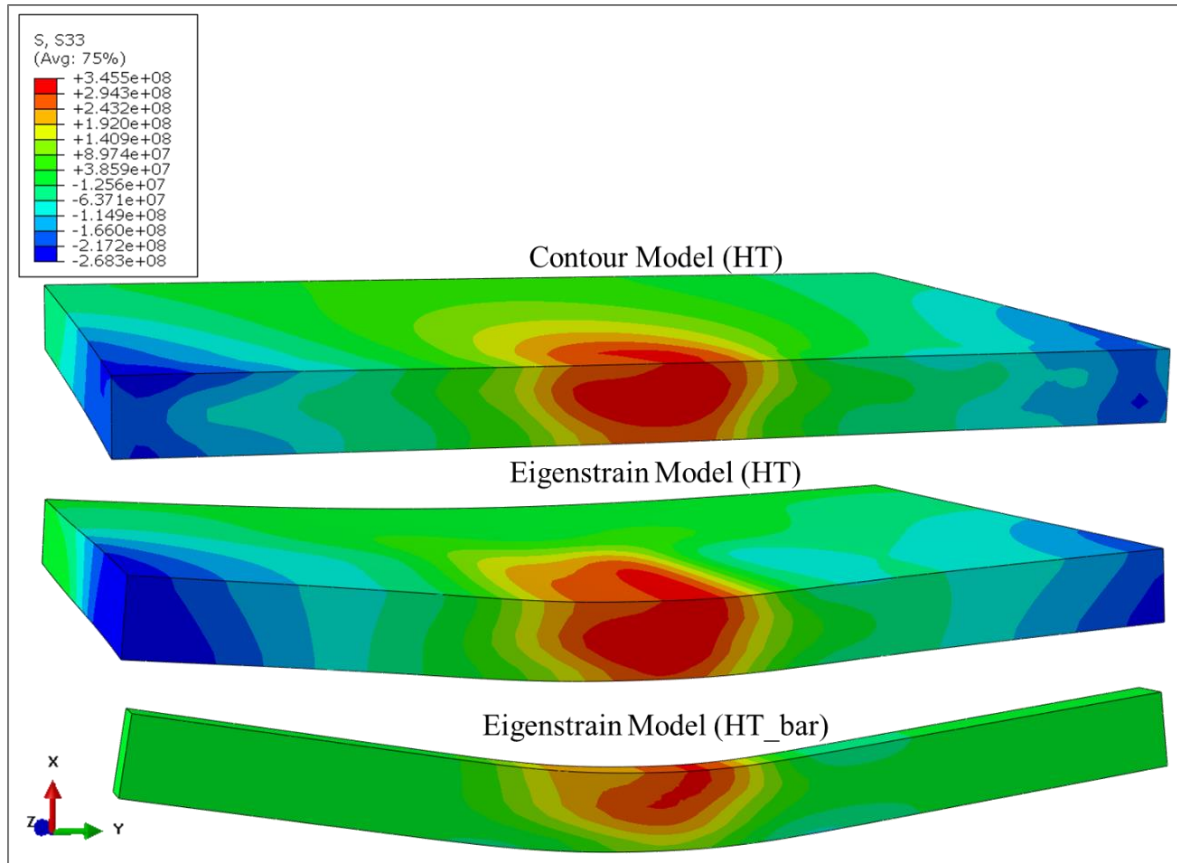


Figure 8. Distribution of longitudinal residual stress (Pa), obtained using eigenstrain reconstruction and contour methods, in heat-treated plate and bar models. Deformations are magnified with a scale factor of 10.

Figure 10 illustrates profile distributions of the through-thickness average of residual stresses in eigenstrain models of as-welded and heat-treated specimens and the results are compared with contour method calculations. Results show very good agreement in both weld zone and edge parts of the plate. Compressive and tensional longitudinal residual stresses appear as a result of eigenstrains in and around the weld zone.

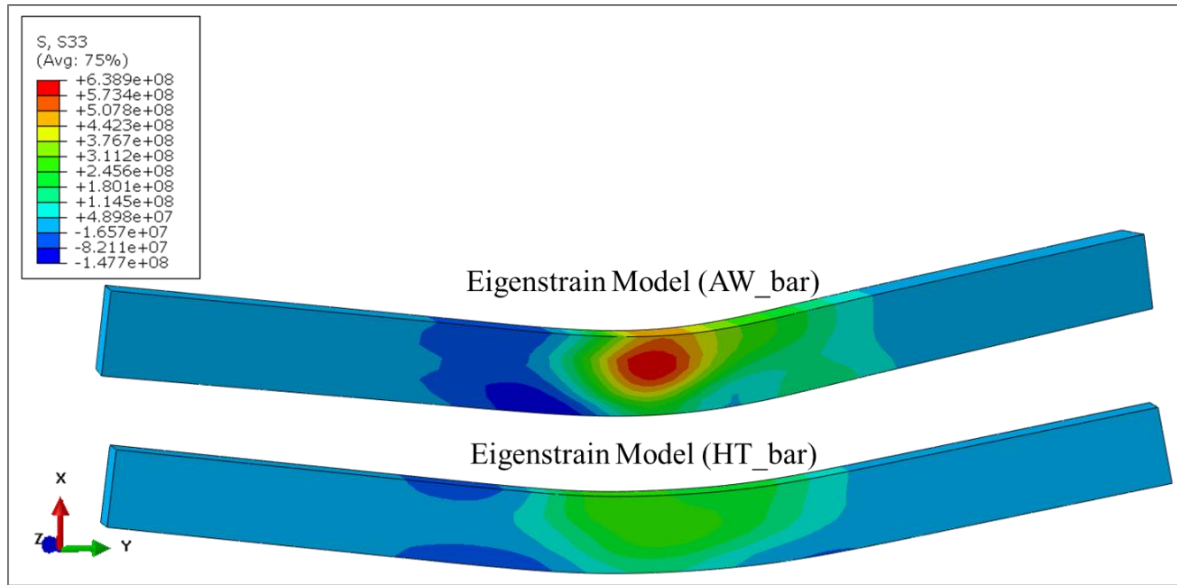


Figure 9. Comparison of distribution of longitudinal residual stress (Pa), obtained using eigenstrain reconstruction method, in as-welded and heat-treated bar models. Deformations are magnified with a scale factor of 10.

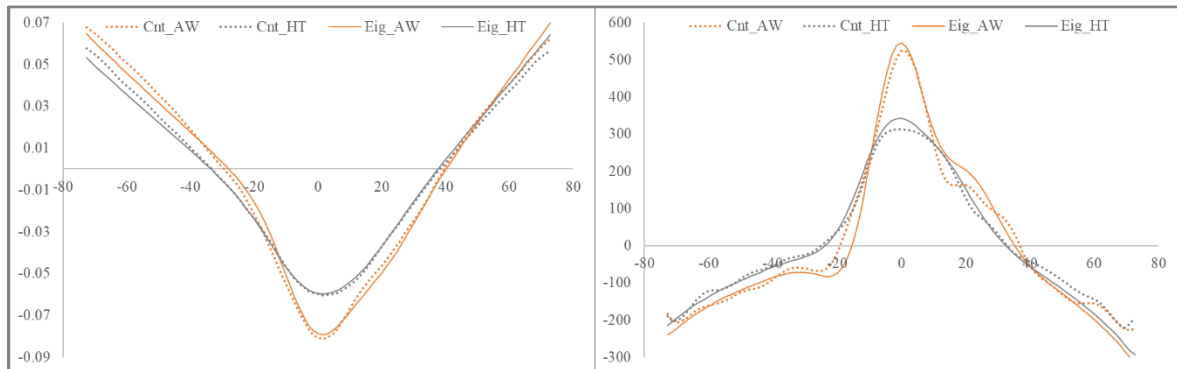


Figure 10. Profile distribution of the through-thickness average of displacement (*millimetres* - left) and longitudinal residual stress (*MPa* - right), obtained using eigenstrain reconstruction and contour methods, on the cut surface of the as-welded and heat-treated plate models.

Comparison of through thickness average of longitudinal residual stresses calculated by solving inverse eigenstrain problem in plate and bar models is given in Figure 11. Tensional residual stresses in the weld zone have lower magnitude in the heat-treated plate model, but

there is not a significant change on the compressive residual stresses at the edge parts. The effect of un-welded part of the plate on formation of compressive residual stresses can be seen clearly on the right graph illustrated in Figure 11. The forces related to the stress should balance each other, and compressive residual stresses have a high influence on creation of that balance in non-uniform plate model. In the case of bar model, which behaves like a uniform weld design, the balance is not satisfied by a solid part that does not include permanent plastic strains and accordingly the distortion is increased. Similar to the results proposed by Ahn et al. [29], longitudinal residual stresses along the transversal direction are composed of tensional stresses around the weld beam and they get vanished away from this field.

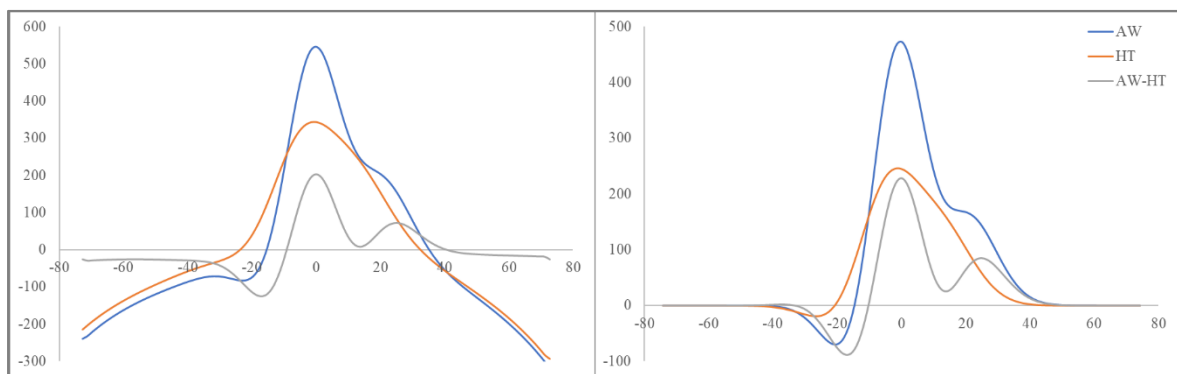


Figure 11. Comparison of profile distribution of the through-thickness average of longitudinal residual stress (MPa), obtained using eigenstrain reconstruction method, on the cut surface of as-welded (left) and heat-treated (right) plate and bar models.

Weld distortion is determined by perimeter measurements of CMM on both plate and bar specimens. The data corresponding to the bottom surface of specimens and the model are extracted for creating profile plots of weld distortion. Results of the distortion measurements and distortions calculated using eigenstrain model are given in Figure 12. Eigenstrain model

calculations show good agreement with coordinate measurements. In the given plots, centre of all distortion data is set to zero point.

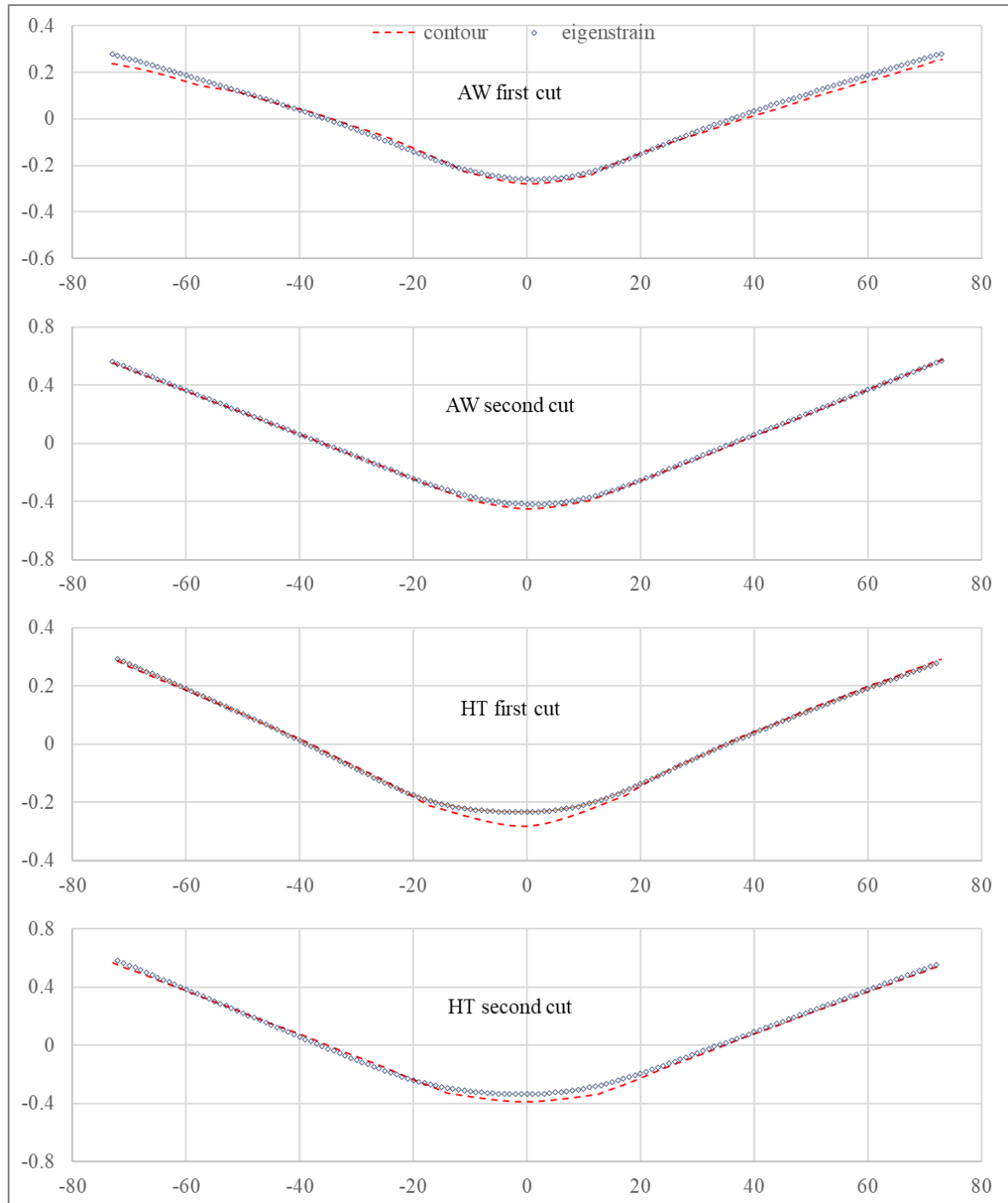


Figure 12. Comparison of transversal weld distortions (*millimetres*), obtained using eigenstrain reconstruction model (eigenstrain) and contour measurements (contour), after first (plate model) and second (bar model) cuts of as-welded (AW) and heat-treated (HT) models.

Distortion calculated in Plane A after first and second cuts in as-welded and heat-treated models are given in Figure 13, where all profile plots of distortion are centred to zero, to show the difference between uniform and non-uniform weld designs. The rise of weld distortion after the second cut can be observed clearly in bar model. In addition, the effect of post weld heat treatment process on weld distortion can be seen clearly. Degree of the weld distortion decreases slightly while bottom part of the model gets a wider curve.

The distortions before the first cut that are predicted by the model shows perfectly good match with contour measurements accomplished before the first cut. They are not included in the plots because distortions in the transversal direction are not influenced by the first cut. Distortions after the first cut represented in the previous figures can be stated to be the same with the distortions before the first cut.

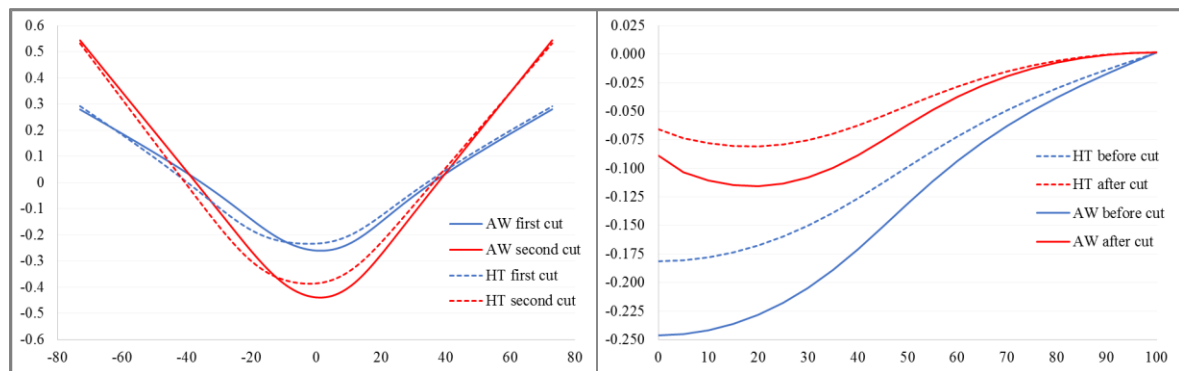


Figure 13. Comparison of transversal distortions in Plane A (left - *millimetres*) and longitudinal weld distortions in Plane C (right - *millimetres*), obtained using eigenstrain reconstruction model, after first and second cuts of as-welded (AW) and heat-treated (HT) models.

Solving multi-component eigenstrain problem using two-dimensional distribution data allowed determination of longitudinal residual stresses and distortion in the whole body.

Residual stresses in plate model are verified by contour method calculations and distortion in plate and bar models are verified by CMM measurements. Therefore, this verified model can be used to predict distortion along the longitudinal direction in Plane C. Longitudinal weld distortion in as-welded and heat-treated models determined using eigenstrain reconstruction process before and after the first cut are illustrated in Figure 13. Results show that weld distortion in this direction is relaxed after the first cut. In both cases, heat-treated model has less distortion.

In this study, weld feed material and base plate has the same chemical composition. Accordingly, investigations on misorientation and inverse pole figure maps obtained from EDM cut surfaces of as-welded and heat-treated specimens, which are illustrated in Figures 14 and 15, are done based on this fact. Grains of weld feed material in the weld zone have larger size when compared to base plate. In addition, larger grains are observed in regions closer to the surface. The reason of the difference between grain sizes is rapid cooling and solidification of the weld feed material. This zone of as-welded and heat-treated specimens seem to have high longitudinal residual stress where longitudinal component of eigenstrains have highest negative magnitude.

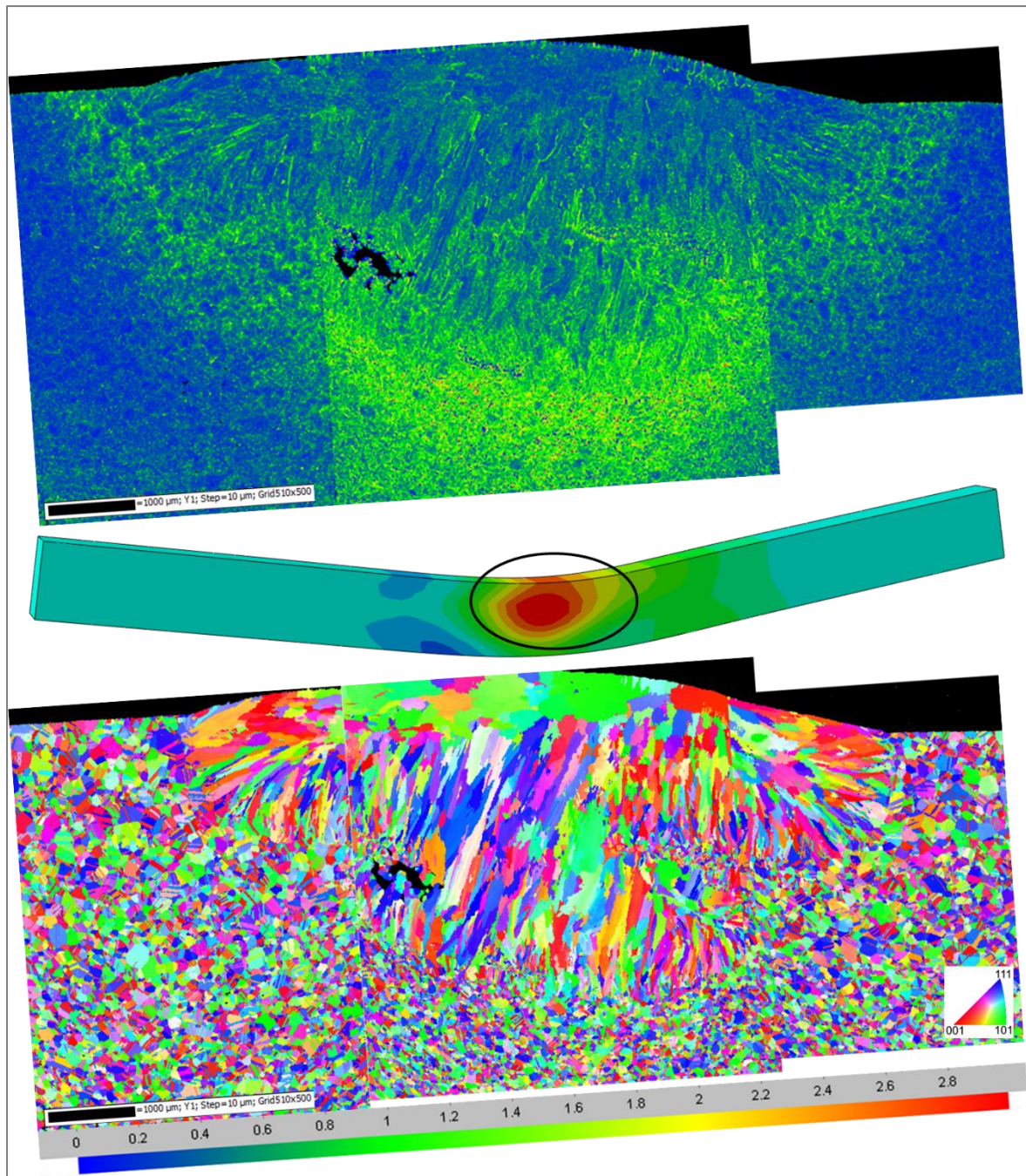


Figure 14. Misorientation and inverse pole figure maps from weld zone of EDM cut surface (Plane A) of as-welded bar specimen.

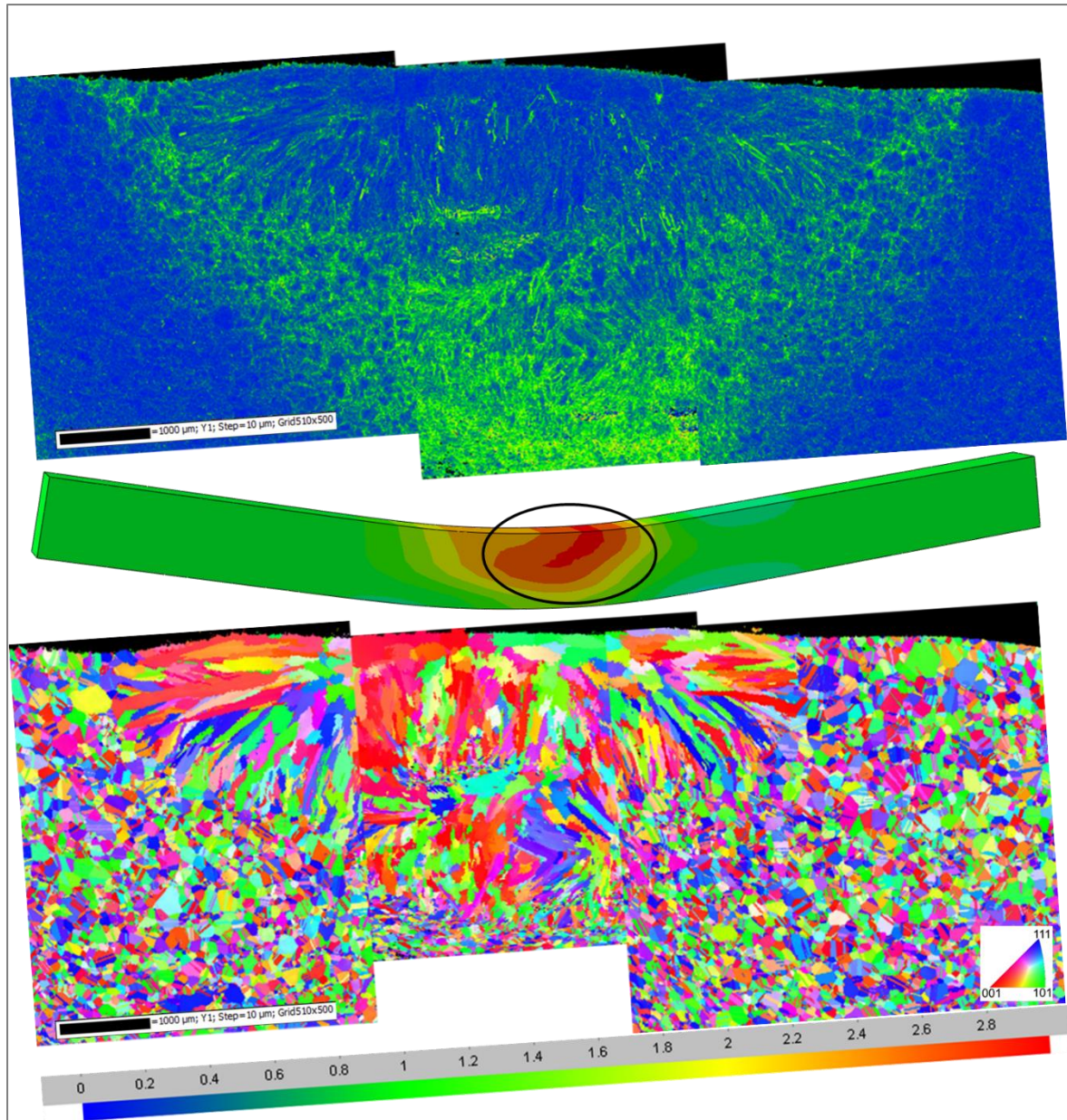


Figure 15. Misorientation and inverse pole figure maps from weld zone of EDM cut surface (Plane A) of heat-treated specimen.

In the boundary between the high magnitude eigenstrain zone and outer parts of the base material, degree of misorientation gets higher. Results show that, heat-treatment process has a reducing effect on the degree of misorientations. According to the observations, it can be stated that boundaries of high magnitude eigenstrain zone matches with boundaries of misorientations.

5. CONCLUSION

Energy demand of the world increases rapidly while the majority of environmental problems are caused by current energy production methods. Renewable energy sources seem to have a high potential, but they are far from fulfilling the current and future energy demand.

Advanced ultra-supercritical technology promises to increase efficiency of coal-powered steam turbines for environmentally friendly energy production by operating at high temperature and pressure conditions. However, components of these turbines are manufactured using fusion welding techniques that cause formation of deformations, defects and residual stresses in the materials. These weak spots in and around weld joints create high risk while operating at harsh conditions. This study provides a new computational method for having a better understanding about the most critical section of components of advanced ultra-supercritical steam turbines.

Capabilities of previously proposed multi-component iterative method [23] are improved by inclusion of displacement data in the second dimension. This increased accuracy of the eigenstrain reconstruction process and allowed verification of the model in terms of experimental distortion data. Residual stresses calculated using plate models have good agreement with experimental results of the contour method. Distortions determined using both plate and bar models are also in good agreement with experimental contour measurements. After two stage verification, it can be concluded that permanent plastic strains (eigenstrains) have a major effect on weld distortions.

Results proved that main source of welding residual stress and weld distortion are the eigenstrains formed in the weld zone. The good fit of distortion in bar models with

experimental measurements improved the reliability of this conclusion, because, after the cutting process, the same eigenstrain field formed during the welding process remained in the bar model. They are the only source of weld distortion and the weld distortion is increased in the bar model like the experimental observation.

The most important property of the proposed modelling technique is that the verified eigenstrain distribution can be used for further investigations. In an example application of this property, distortion along the longitudinal direction is determined using the calculated eigenstrain distribution. This implementation shows that the proposed iterative eigenstrain reconstruction model can make reliable predictions about deformations in the whole material when experimental data about the in-volume deformations is not available. Microscopy analyses showed that the boundaries of eigenstrain fields are consistent with misorientation and inverse pole figure maps.

ACKNOWLEDGEMENTS

This project has received funding from the European Union's Horizon 2020 research and innovation programme under the Marie Skłodowska-Curie grant agreement No 794957 and EPSRC through grant EP/S005072/1 Strategic Partnership in Computational Science for Advanced Simulation and Modelling of Engineering Systems (ASiMoV)

REFERENCES

- [1] Furtado HC, Le May I. High temperature degradation in power plants and refineries. *Mater Res* 2004;7:103–10. doi:10.1590/S1516-14392004000100015.

- [2] Withers PJ, Bhadeshia HKDH. Residual stress. Part 2 – Nature and origins. *Mater Sci Technol* 2001;17:366–75. doi:10.1179/026708301101510087.
- [3] Masubuchi K. Models of Stresses and Deformation Due to Welding—A Review. *JOM J Miner Met Mater Soc* 1981;33:19–23. doi:10.1007/BF03339550.
- [4] Tian L, Luo Y, Wang Y, Wu X. Prediction of transverse and angular distortions of gas tungsten arc bead-on-plate welding using artificial neural network. *Mater Des* 2014;54:458–72. doi:10.1016/j.matdes.2013.08.082.
- [5] Li Y, Zhao Y, Li Q, Wu A, Zhu R, Wang G. Effects of welding condition on weld shape and distortion in electron beam welded Ti2AlNb alloy joints. *Mater Des* 2017;114:226–33. doi:10.1016/j.matdes.2016.11.083.
- [6] Okano S, Mochizuki M. Transient distortion behavior during TIG welding of thin steel plate. *J Mater Process Technol* 2017;241:103–11. doi:10.1016/j.jmatprotec.2016.11.006.
- [7] Bajpei T, Chelladurai H, Ansari MZ. Experimental investigation and numerical analyses of residual stresses and distortions in GMA welding of thin dissimilar AA5052-AA6061 plates. *J Manuf Process* 2017;25:340–50. doi:10.1016/j.jmapro.2016.12.017.
- [8] Montevecchi F, Venturini G, Grossi N, Scippa A, Campatelli G. Finite Element mesh coarsening for effective distortion prediction in Wire Arc Additive Manufacturing. *Addit Manuf* 2017;18:145–55. doi:10.1016/j.addma.2017.10.010.
- [9] Luo Y, Murakawa H, Ueda Y. Prediction of welding deformation and residual stress by elastic FEM based on inherent strain. *日本造船学会論文集* 1998;183:323–33.
- [10] Wang J, Yuan H, Ma N, Murakawa H. Recent research on welding distortion prediction in thin plate fabrication by means of elastic FE computation. *Mar Struct* 2016;47:42–59. doi:10.1016/j.marstruc.2016.02.004.

- [11] Park J ung, An G. Prediction of the welding distortion of large steel structure with mechanical restraint using equivalent load methods. *Int J Nav Archit Ocean Eng* 2017;9:315–25. doi:10.1016/j.ijnaoe.2016.11.002.
- [12] Fitzpatrick ME, Lodini A. Analysis of Residual Stress by Diffraction Using Neutron and Synchrotron Radiation. vol. 14. 2003. doi:10.1088/0957-0233/14/9/703.
- [13] Javadi Y, Akhlaghi M, Najafabadi MA. Using finite element and ultrasonic method to evaluate welding longitudinal residual stress through the thickness in austenitic stainless steel plates. *Mater Des* 2013;45:628–42. doi:10.1016/j.matdes.2012.09.038.
- [14] Uzun F, Bilge AN. Ultrasonic Investigation of the Effect of Carbon Content in Carbon Steels on Bulk Residual Stress. *J Nondestruct Eval* 2015;34. doi:10.1007/s10921-015-0284-x.
- [15] Prime MB. Cross-Sectional Mapping of Residual Stresses by Measuring the Surface Contour After a Cut. *J Eng Mater Technol* 2001;123:162. doi:10.1115/1.1345526.
- [16] Kartal M, Turski M, Johnson G, Fitzpatrick ME, Gungor S, Withers PJ, et al. Residual stress measurements in single and multi-pass groove weld specimens using neutron diffraction and the contour method. *Mater Sci Forum* 2006;524–525:671–676. doi:10.4028/www.scientific.net/MSF.524-525.671.
- [17] Prime MB, Gnäupel-Herold T, Baumann JA, Lederich RJ, Bowden DM, Sebring RJ. Residual stress measurements in a thick, dissimilar aluminum alloy friction stir weld. *Acta Mater* 2006;54:4013–21. doi:10.1016/j.actamat.2006.04.034.
- [18] Traore Y, Paddea S, Bouchard PJ, Gharghoury MA. Measurement of the Residual Stress Tensor in a Compact Tension Weld Specimen. *Exp Mech* 2013;53:605–18. doi:10.1007/s11340-012-9672-7.
- [19] Toparli MB, Fitzpatrick ME, Gungor S. Improvement of the Contour Method for Measurement of Near-Surface Residual Stresses from Laser Peening. *Exp Mech*

- 2013;53:1705–18. doi:10.1007/s11340-013-9766-x.
- [20] Zabeen S, Preuss M, Withers PJ. Residual stresses caused by head-on and 45° foreign object damage for a laser shock peened Ti-6Al-4V alloy aerofoil. *Mater Sci Eng A* 2013;560:518–27. doi:10.1016/j.msea.2012.09.097.
 - [21] DeWald AT, Hill MR. Multi-Axial Contour Method for Mapping Residual Stresses in Continuously Processed Bodies. *Exp Mech* 2006;46:473–90. doi:10.1007/s11340-006-8446-5.
 - [22] Kartal ME, Kang YH, Korsunsky AM, Cocks ACF, Bouchard JP. The influence of welding procedure and plate geometry on residual stresses in thick components. *Int J Solids Struct* 2016;80:420–9. doi:10.1016/j.ijsolstr.2015.10.001.
 - [23] Uzun F, Korsunsky AM. On the identification of eigenstrain sources of welding residual stress in bead-on-plate inconel 740H specimens. *Int J Mech Sci* 2018;145:231–45. doi:doi.org/10.1016/j.ijmecsci.2018.07.007.
 - [24] Ahn J, He E, Chen L, Wimpory RC, Dear JP, Davies CM. Prediction and measurement of residual stresses and distortions in fibre laser welded Ti-6Al-4V considering phase transformation. *Mater Des* 2017;115:441–57. doi:10.1016/j.matdes.2016.11.078.
 - [25] Mura T. *Micromechanics of Defects in Solids*. Dordrecht: Netherlands: Kluwer Academic Publishers; 1982.
 - [26] Korsunsky AM. *A Teaching Essay on Residual Stresses and Eigenstrains*. Oxford, United Kingdom: Butterworth-Heinemann; 2017.
 - [27] Korsunsky AM. Power Law Multi-Scaling of Material Strength 2005:1–14.
 - [28] Hosseinzadeh F, Kowal J, Bouchard PJ. Towards good practice guidelines for the contour method of residual stress measurement. *J Eng* 2014. doi:10.1049/joe.2014.0134.
 - [29] Ahn J, He E, Chen L, Wimpory RC, Kabra S, Dear JP, et al. FEM prediction of

welding residual stresses in fibre laser-welded AA 2024-T3 and comparison with experimental measurement. *Int J Adv Manuf Technol* 2018;95:4243–63.
doi:10.1007/s00170-017-1548-7.